Electronic structure of rare-earth impurities in GaAs and GaN

A. Svane,[1] N. E. Christensen,[1] L. Petit,[2] Z. Szotek,[3] and W. M. Temmerman[3]
[1]*Department of Physics and Astronomy, University of Aarhus, DK-8000 Aarhus C, Denmark*
[2]*Computer Science and Mathematics Division, and Center for Computational Sciences, Oak Ridge National Laboratory, Oak Ridge, Tennessee 37831, USA*
[3]*Daresbury Laboratory, Daresbury, Warrington WA4 4AD, United Kingdom*
(Received 10 March 2006; revised manuscript received 21 August 2006; published 6 October 2006)

The electronic structures of substitutional rare-earth (RE) impurities in GaAs and cubic GaN are calculated. The total energy is evaluated with the self-interaction corrected local spin density approximation, by which several configurations of the open $4f$ shell of the rare-earth ion are investigated. The defects are modeled by supercells of type $RE\mathrm{Ga}_{n-1}\mathrm{As}_n$, for $n=4$, 8, and 16. The preferred defect is the rare-earth substituting Ga, for which case the rare-earth valency in intrinsic material is found to be trivalent. The $3+\rightarrow 2+$ f-level is found above the theoretical conduction band edge in all cases and within the experimental gap only for Eu, Tm, and Yb in GaAs and for Eu in GaN. The exchange interaction of the rare-earth impurity with the states at both the valence band maximum and the conduction band minimum is weak, one to two orders of magnitude smaller than that of Mn impurities. Hence the coupling strength is insufficient to allow for ferromagnetic ordering of dilute impurities, except at very low temperatures.

DOI: 10.1103/PhysRevB.74.165204 PACS number(s): 75.50.Pp, 71.55.Eq, 71.70.Gm, 71.27.+a

I. INTRODUCTION

The technology of electronics exploiting both charge- and spin-degrees of freedom of carriers is a rapidly developing research field.[1,2] Diluted magnetic semiconductors (DMS) are good candidates for new generations of fast, low dissipation, nonvolatile integrated information and processing devices. In particular, ferromagnetic semiconductors offer a unique combination of magnetic, semiconducting, and optical properties, together with compatibility with existing microelectronics technology. In the longer term, the long electron lifetimes in semiconductors coupled with their strong interplay with nuclear spins might be exploited for quantum computing.[3] Several reports of ferromagnetically ordered DMS at room temperature (see, e.g., Refs. 4 and 5 and references therein) pose questions of fundamental importance as to the nature of magnetic interactions in these materials.[6–12]

Most efforts have investigated Mn and other $3d$ impurities in III–V and II–VI hosts, but recently also the discovery of high temperature ferromagnetism[13,14] in diluted Gd-doped GaN has gained considerable interest, implying that rare-earth (RE) ions may become a viable alternative to transition metals for spintronics applications. In addition, rare-earth doping of wide-gap semiconductors such as GaN and ZnO is an active research area in itself due to the possibility of achieving tunable light emission,[15] arising from intra-f-shell optical transitions.

The theoretical modeling of solids containing rare-earths poses severe problems due to the correlated nature of the f electrons in the incompletely filled $4f$ shell. A description in terms of bands, as implemented in the conventional local spin density (LSD) approximation[16,17] invoked in the framework of density-functional theory,[18] leads to a large overestimation of the contribution of f-electrons to bonding and hence to too small lattice constants. In addition, even if the band structures of LSD have no formal interpretation, they are often used as guidelines for what the elementary electron excitations of the solid are, but in the case of f-electron materials the approach is particularly poor. The f derived states appear as a set of narrow bands situated close to the Fermi level, while experiments reveal their localized nature as atomic multiplet features over a broad energy range.[19] The luminescence of rare-earth impurities in semiconducting hosts is well-interpreted in terms of $f^n \rightarrow f^n$ transitions in ionic models perturbed by the crystal fields of the host, see, e.g., Refs. 20 and 21. However, charge transitions like $f^n \rightarrow f^{n\pm 1}$ are more difficult to calculate due to the significant screening processes involved. The energetics of rare-earth related defects in GaN have been studied by the LSD method treating the f-electrons as corelike, assuming trivalent configurations.[22] The LDA+U method has been invoked for the study of Er:GaN defects,[23] where the Coulomb U parameter is used to push unoccupied f-states high into the conduction state region. For Gd, due to the half-filled shell and the large exchange splitting, the LSD provides a reasonably accurate description.[24]

The present work undertakes a systematic theoretical investigation of the electronic structure of rare-earth dopants in GaAs and GaN, both in the zinc-blende crystal structure, using the self-interaction corrected (SIC) local spin density method.[25] Total energy calculations reveal Ga substitution as the most favorable rare-earth defect, with the rare-earth ion taking the isoelectronic trivalent configuration in all cases studied. The effect of the exchange interaction of the rare-earth ion with the host states at the valence band maximum (VBM) and conduction band minimum (CBM) is calculated, and is found surprisingly weak given the large spin moment formed on the rare-earth ion. A significant hybridization effect between the unoccupied f-states and the CBM states is observed. Furthermore, the position of the divalent acceptor level $\epsilon(0/-)$ is calculated and found outside the theoretical band gap, i.e., appearing as a resonance in the conduction bands. However, the $\epsilon(0/-)$ level falls inside the experimen-

tal band gap for Eu in GaN and for Eu, Tm, and Yb in GaAs.

The SIC-LSD method, employed in the present work, constitutes an extension of the conventional LSD approximation by correcting for the spurious self-interaction of individual electrons, which is inherent in the LSD approximation. For rare-earth atoms the self-interaction correction allows for a localization of the f-electrons. In this way the atomic limit of the rare-earth f shell is implemented in conjunction with the itinerant limit of the other rare-earth valence electrons and the valence electrons of the semiconducting host. In particular, the ground state configuration of the rare-earth f-shell is determined from comparison of the total energy corresponding to different valency scenarios, as has already been shown in several applications to rare-earth solids,[26–28] including pressure induced valence transitions.[29–31] Not included in the present theory is the full multideterminant description of multiplet formation.

In Sec. II of the present paper we outline the theoretical aspects of the present work, notably the SIC-LSD total energy method as well as other calculational details. In Sec. III the results are presented for defect formation energies, magnetic interactions, and valency transition energies. Section IV contains the summary and conclusions of this work.

II. THEORY

A. The SIC-LSD total energy method

The total energy functional of the LSD approximation is renowned for its chemical accuracy in describing conventional solids with weakly correlated electrons.[16,17] The self-interaction correction is included to facilitate an accurate description of the localized f electrons of rare-earths. Specifically, the SIC-LSD[25] total energy functional is obtained from the LSD as

$$E^{SIC\text{-}LSD} = E^{LSD} + \Delta E_{sic} + E_{so}, \tag{1}$$

$$\Delta E_{sic} = -\sum_{\alpha}^{occ.} \delta_{\alpha}^{SIC}, \tag{2}$$

$$E_{so} = \sum_{\alpha}^{occ.} \epsilon_{\alpha}^{so}, \tag{3}$$

where α labels the occupied states and δ_{α}^{SIC} is the self-interaction correction for state α. As usual, E^{LSD} can be decomposed into a kinetic energy, T, a Hartree energy, U, the interaction energy with the atomic ions, V_{ext}, and the exchange and correlation energy, E_{xc}.[18] The self-interaction is defined as the sum of the Hartree interaction and the exchange-correlation energy for the charge density of state α:

$$\delta_{\alpha}^{SIC} = U[n_{\alpha}] + E_{xc}[n_{\alpha}]. \tag{4}$$

For itinerant states, δ_{α}^{SIC} vanishes identically, while for localized (atomiclike) states the self-interaction may be appreciable. This correction constitutes a negative energy contribution for an f-electron to localize, which then competes with the band formation energy gained by the f-electron if allowed to delocalize and hybridize with the available conduction states. In rare-earths the self-interaction correction ranges from $\delta_{\alpha}^{SIC} \sim 0.8$ eV per f-electron in Ce to $\delta_{\alpha}^{SIC} \sim 1.5$ eV per f-electron in Yb, reflecting the contraction of the f-orbitals through the series. The volume dependence of δ_{α}^{SIC} is rather weak, hence the overbinding of the LSD approximation for narrow band states is reduced when localization is allowed. The last term in Eq. (1) is the spin-orbit energy, where for each occupied state α

$$\epsilon_{\alpha}^{so} = \langle \psi_{\alpha} | \xi(\vec{r}) \vec{l} \cdot \vec{s} | \psi_{\alpha} \rangle \tag{5}$$

is added to the energy functional. We employ the atomic spheres approximation, whereby the crystal volume is divided into slightly overlapping atom-centered spheres of a total volume equal to the actual volume. In Eq. (5), the angular momentum operator, $\vec{l} = \vec{r} \times \vec{p}$, is defined inside each atomic sphere, with $\vec{r}$ given as the position vector from the sphere center. The spin-orbit interaction couples the band Hamiltonian for the spin-up and spin-down channels, i.e., a doubled secular problem must be solved. Other relativistic effects are automatically included by solving the scalar-relativistic radial equation inside spheres. The spin-orbit parameter,

$$\xi(r) = -\frac{2}{c^2}\frac{dV}{dr}$$

in atomic Rydberg units, is calculated from the self-consistent potential. The SIC-LSD energy functional in Eq. (1) appears to be a functional of all the one-electron orbitals, but can in fact be viewed as a functional of the total (spin) density alone, as discussed in Ref. 32.

The advantage of the SIC-LSD energy functional is that it allows for different valency scenarios to be explored. By assuming atomic configurations with different total numbers of localized states, self-consistent minimization of the total energy leads to different local minima of the same functional, $E^{SIC\text{-}LSD}$ in Eq. (1), and hence their total energies may be compared. The configuration with the lowest energy defines the ground state configuration. Note that if no localized states are assumed, $E^{SIC\text{-}LSD}$ coincides with the conventional LSD functional, i.e., the Kohn-Sham minimum of the E^{LSD} functional is also a local minimum of $E^{SIC\text{-}LSD}$. The interesting question is, whether competing minima with a finite number of localized states exist. This is usually the case in f-electron systems[26] and some $3d$ transition metal compounds,[33] where the respective f and d orbitals are sufficiently confined in space to benefit appreciably from the SIC.

The SIC-LSD still considers the electronic structure of the solid to be built from individual one-electron states, but offers an alternative description to the Bloch picture, namely in terms of periodic arrays of localized atom-centered states (i.e., the Heitler-London picture in terms of Wannier orbitals). Nevertheless, there still exist states which will never benefit from the SIC. These states retain their itinerant character of the Bloch form and move in the effective LSD potential. This is the case for the host valence band states in the

systems studied here. The SIC-term only affects the rare-earth ions. The resulting many-electron wave function will consist of both localized and itinerant states. The nominal valency of a rare-earth ion is defined as the number of valence electrons available for band formation:

$$N_{val} = Z - N_{core} - N_{SIC},$$

where Z is the nuclear charge, N_{core} the number of core electrons, and N_{SIC} the number of self-interaction corrected f-electrons.

In contrast to the LSD Kohn-Sham equations, the SIC electron states, which minimize $E^{SIC\text{-}LSD}$, experience different effective potentials. This implies that to minimize $E^{SIC\text{-}LSD}$, it is necessary to explicitly ensure the orthonormality of the one-electron wave functions by introducing a Lagrangian multipliers matrix. Furthermore, the total energy is not anymore invariant with respect to a unitary transformation of the one-electron wave functions. Both of these aspects make the energy minimization more demanding to accomplish than in the LSD case. The electron wave functions are expanded in linear-muffin-tin-orbital (LMTO) basis functions,[34] and the energy minimization problem becomes a nonlinear optimization problem in the expansion coefficients. Further details of the present implementation can be found in Ref. 35.

B. Calculational details

Alloys of GaAs (or GaN) and rare-earth ions of the type $RE_xGa_{1-x}As$ ($RE_xGa_{1-x}N$) and RE_xGaAs_{1-x} (RE_xGaN_{1-x}) were considered by supercell modeling, and total energies evaluated for $x=1/4$, $1/8$, and $1/16$. The experimental lattice constants of pure GaAs and GaN in the zinc-blende structure were used ($a=5.65$ Å for GaAs, $a=4.45$ Å for GaN), i.e., the effects of lattice expansion with doping were assumed negligible. The cubic form of GaN (rather than the more common wurtzite structure) was considered for computational convenience. Previous studies of defects in GaN have revealed quite close agreement between defect levels in the two crystal structures,[36] albeit symmetry related splittings occur. The cubic structure can be stabilized by incorporation of transition metal impurities,[37] but this issue is not pursued here. The atomic positions were kept fixed in all calculations, except for a few test cases discussed in the next section, i.e., no systematic study of the effects of relaxations of nearest neighbors of the impurities were attempted. Experimentally, for Er-doped GaN the Er-N distance has been found ~10% larger than the pure host Ga-N bond length.[38]

The itinerant states were sampled using 95, 22, and 14 k-points in the irreducible wedge of the Brillouin zone of the $x=1/4$, $1/8$, and $1/16$ supercells, respectively. In GaAs, the $3d$ semicore states of Ga and As were treated self-consistently in a separate energy panel, which also included the $5s$ and $5p$ semicore states of the rare-earth. In the case of the GaN host, the best description is obtained with only the $5s$ semicore states of the rare-earth impurity treated in the separate semicore panel. Due to the smaller lattice constant, there is a pronounced interaction between the N $2s$, $2p$ states and the Ga $3d$ and rare-earth $5p$ states, for which reason the latter were treated as valence electrons to include their hybridization into the GaN valence bands.

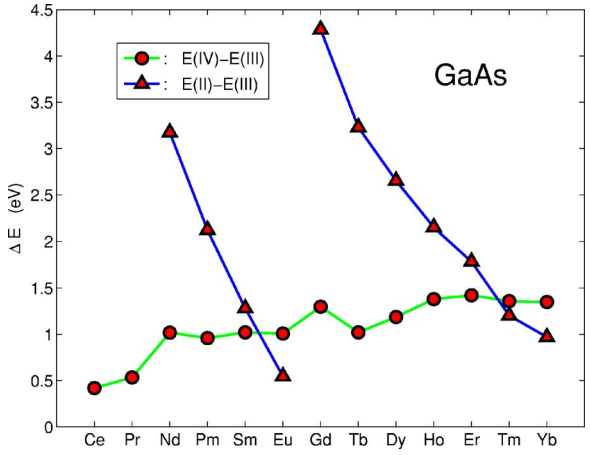

FIG. 1. (Color online) The energy difference between tetravalent and trivalent rare-earth impurities substituting for Ga in GaAs (circles), and for selected cases between divalent and trivalent ions (triangles). The calculations were performed for supercells corresponding to rare-earth concentration $x=1/16$. The positive sign implies that the trivalent configuration is the ground state.

III. RESULTS AND DISCUSSION

A. Cohesive properties

Figures 1 and 2 show the energy differences calculated for trivalent, divalent, and tetravalent configurations of the rare-earth impurities, in GaAs and GaN, respectively, at concentration $x=1/16$. The rare-earth ion is taken to substitute for Ga. The preferred valency is seen to be trivalent for all rare-earth impurities in GaAs and GaN, in good accord with the trivalency of the Ga atom which the rare-earth replaces, and with the interpretaion of photoluminescence experiments on rare-earth doped GaN.[15] In particular, the Eu and Yb impurities remain trivalent (by a margin of more than 0.5 eV) in

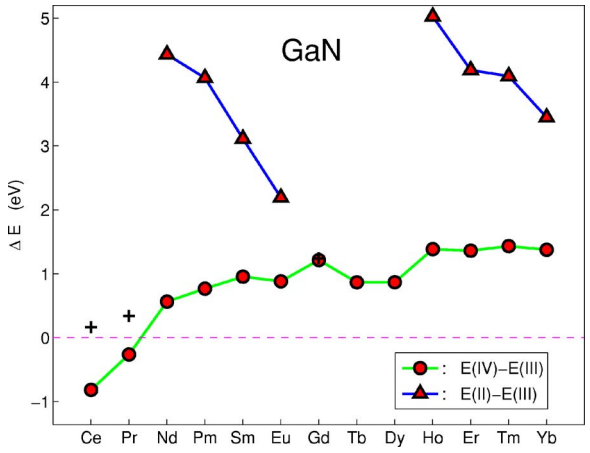

FIG. 2. (Color online) The energy difference between tetravalent and trivalent rare-earth impurities substituting for Ga in cubic GaN (circles), and for selected cases between divalent and trivalent ions (triangles). The calculations were performed for supercells corresponding to rare-earth concentration $x=1/16$. The results marked with "+" include relaxations of nearest-neighbor N atoms, showing the switch to trivalent ground state for Ce and Pr when relaxations are included.

spite of the tendency of these elements to become divalent, e.g., in the elemental metallic phase. Luminescence experiments show that Eu in GaN is trivalent,[39] although there have been indications of divalent Eu in the surface region of Eu-doped GaN.[40,41]

In GaAs, the valence energy difference is almost independent of concentration, except for Ce, for which case, at concentrations $x=1/4$ and $1/8$ the preferred configuration is f^0 (tetravalent). This means that f-band formation is favored for Ce impurities at this large concentration, i.e., instead of having one localized f-electron on each Ce atom, a narrow f-band is formed close to the conduction band minimum and filled with one electron leading to a metallic alloy. However, in the most diluted case studied here, $x=1/16$, the localization of one f-electron on each Ce is more favorable, leading to a ground state with cerium ions in the trivalent f^1 configuration and a semiconducting alloy, which we hence assume to prevail also at Ce concentrations of even lower value.

In GaN both Ce and Pr at first are found to be tetravalent, even at $x=1/16$, i.e., again implying the formation of narrow f-bands straddling the conduction band edge and metallicity. However, effects of relaxations of the nearby host atoms are important. As a check, a similar valency energy difference was calculated for Ce and Pr in GaN with the nearest-neighbor N atoms moved 10% of the bond length away from Ce (Pr) (see +'s in Fig. 2), and indeed the trivalent configuration in this case had a lower energy (by 0.14 eV for Ce and 0.27 eV for Pr) than the tetravalent configuration. For Gd the effect of relaxations on the valency energy difference is a modest increase by 0.03 eV in favor of the trivalent configuration, barely visible on the figure. Experimentally, dilute rare earths in GaN are all observed in the trivalent state, in particular the rich spectrum of GaN:Pr can only be interpreted in terms of Pr^{3+} ions.[42] The detailed analysis of the localization-delocalization transition upon dilution would need to incorporate besides the relaxation of atomic positions in the vicinity of the impurity, also issues of impurity disorder and/or clustering, which is not attempted here.

The trends of the formation energy of charge neutral substitutional rare-earth ions in GaAs and GaN are depicted in Fig. 3. The formation energy is defined as

$$E_{form} = E(RE\mathrm{Ga}_{15}\mathrm{As}_{16}) + \mu_{\mathrm{Ga}} - E(\mathrm{Ga}_{16}\mathrm{As}_{16}) - \mu_{RE}, \quad (6)$$

where the two energies, $E(RE\mathrm{Ga}_{15}\mathrm{As}_{16})$ and $E(\mathrm{Ga}_{16}\mathrm{As}_{16})$, are total energies calculated for the $RE\mathrm{Ga}_{15}\mathrm{As}_{16}$ and $\mathrm{Ga}_{16}\mathrm{As}_{16}$ supercells. μ_{Ga} is the chemical potential for Ga, which depends on the growth conditions of the doped semiconductor. During growth the chemical potentials for Ga and As are constrained by $\mu_{\mathrm{Ga}}+\mu_{\mathrm{As}}=E(\mathrm{GaAs})$. For Ga-rich conditions, excess Ga is assumed to be in the metallic phase (orthorhombic α-Ga, *Cmca* symmetry), i.e., $\mu_{\mathrm{Ga}}=E(\alpha\text{-Ga})$, while for As-rich (N-rich) conditions excess As (N) is assumed to exist as solid As (rhombohedral α-As, symmetry $R\bar{3}m$) and N_2 gas, respectively, i.e., $\mu_{\mathrm{As}}=E(\alpha\text{-As})$ and $\mu_{\mathrm{N}}=\frac{1}{2}E(\mathrm{N}_2)$. Similarly, the chemical potential for the rare-earth depends on the growth conditions. In the case of Ga-rich conditions, it is taken as the total energy for the elemental metallic phase $\mu_{RE}=E(RE)$, likewise calculated with the SIC-LSD method,[26] while for As (N) rich growth conditions, excess rare earth is assumed in the form of the binary pnictide compound (in the rocksalt structure), also calculated with the SIC-LSD method, i.e., $\mu_{RE}=E(REX)-\mu_X$ for $X=\mathrm{As},\mathrm{N}$. The formation energies in Fig. 3 refer to the pnictide-rich growth conditions. The formation energies are seen to exhibit a monotonously decreasing trend through the rare-earth series. The formation energies will be somewhat lowered by relaxations of the host atomic positions in the vicinity of the impurity, which were not considered here. A check of the relaxation effects was performed for Gd in GaN using the LSD approximation as implemented in the full-potential version of the LMTO approach of Ref. 43. This calculation revealed an 11% outward relaxation of the nearest-neighbor N atoms of the Gd impurity, which is in excellent agreement with experimental investigations[38] as well as other theoretical calculations[22,23] for rare earths in GaN. The accompanying release of elastic energy is of the order of 1 eV. The use of the LSD approximation for this particular system is justified by the similarity of the electronic structure of Gd in LSD and SIC-LSD (due to the half-filled f-shell), but cannot be relied upon in general. For Ga-rich conditions, the formation energies exhibit a similar monotonously decreasing trend through the series (not shown).

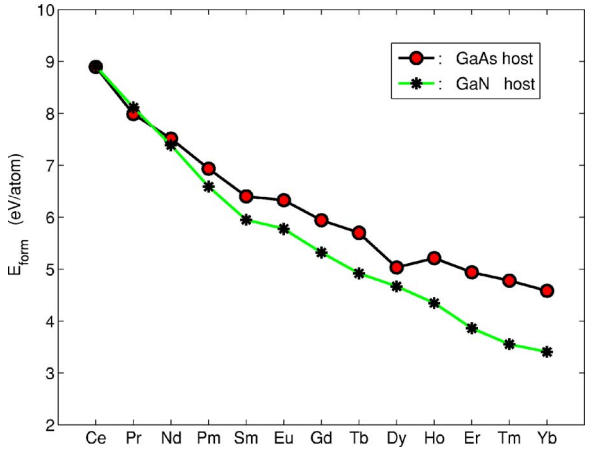

FIG. 3. (Color online) Formation energies [cf. Eq. (6)] for substitutional rare-earth ions in GaAs (circles) and GaN (asterisk) under pnictide-rich conditions (see text for discussions).

A few cases of rare-earth ions substituting for As in GaAs have been considered: Pr, Eu and Tb. For these, the formation energies are substantially higher, namely 12.6, 10.3, and 11.2 eV, respectively, again for As-rich conditions. We conclude that indeed the As-substitution is unfavorable compared to Ga-substitution, as also evidenced by experiments.[15]

In Fig. 4 the electronic density of states is illustrated for the case of Eu in GaN. The calculated gap is 2.0 eV (in the presence of Eu), defined as the separation of the host Γ_8 valence band maximum state and the Γ_6 conduction band minimum state. The figure reveals a sharp resonance inside the gap region originating from the single Eu majority f-state, which is not localized in the f^6 configuration, and hence appears as an unoccupied impurity band state. We discuss this state later, in Sec. III C. The minority Eu f-states

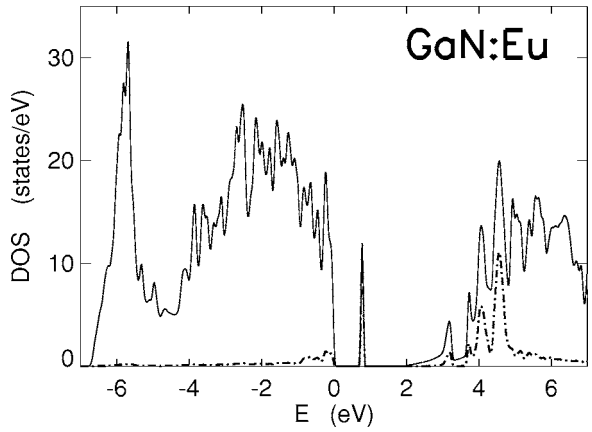

FIG. 4. Electron density of states (DOS) for Eu in GaN ($x=1/16$). Full line shows the total DOS of the $x=1/16$ supercell in units of states per eV and supercell. The dashed line shows the DOS projected onto the Eu site. The zero of energy is placed at the VBM.

are seen to hybridize into the conduction bands 4 to 5 eV above the VBM. The energy position of the localized states are not shown (see discussion in Sec. III D).

B. Magnetic properties

The magnetic moments of the rare-earth impurities in GaAs and GaN are depicted in Fig. 5. Both spin and orbital moments are dominated by the Hund's rule ground state of the rare-earth ion, with generally small contributions from the band states. This leads to the characteristic sinusoidal variation of the orbital moment with antiparallel (parallel) orientation compared to the spin moment in the first (second) half of the rare-earth series. The Hund's rule ground state is represented in the SIC-LSD calculation by localizing the f-states that maximize the spin and orbital moment projection on the z-axis with the same (opposing) sign for more (less) than half filling.

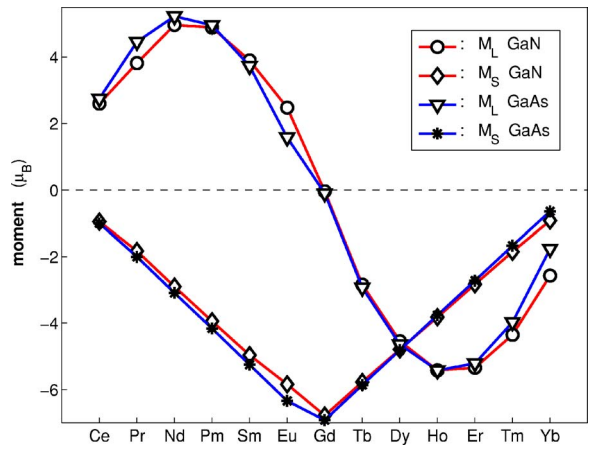

FIG. 5. (Color online) Spin and orbital moments of rare-earth impurities in GaAs and GaN in units of the Bohr magneton, μ_B. The orbital moments ($M_L=L_z\mu_B/\hbar$) are marked with circles (GaN) and triangles (GaAs), while the spin moments ($M_S=g_0S_z\mu_B/\hbar$, where g_0 is the electron gyromagnetic ratio) are shown with diamonds (GaN) and asterisks (GaAs).

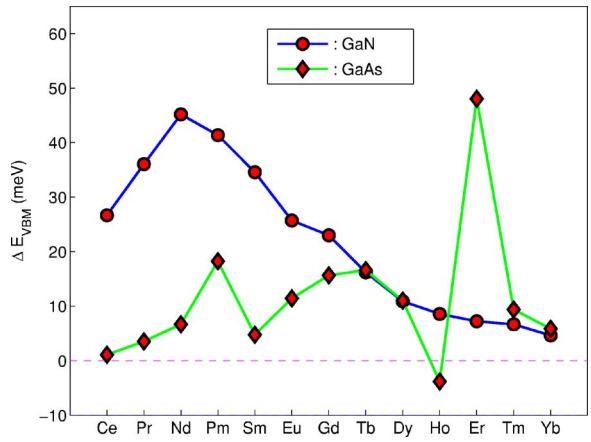

FIG. 6. (Color online) Spin-splitting (in meV) of the electron bands at the valence band maximum for rare-earth dopants in GaN (circles) and GaAs (diamonds) for $x=1/16$. A positive sign implies that the band state with its spin aligned with the rare-earth spin has a lower energy than the state with its spin antiparallel to that of the rare-earth ion. The sign change of the spin-splitting for GaAs at Ho is caused by the mixing in of the unoccupied rare-earth impurity f-bands into the top of the valence band.

The magnetic interaction of the rare-earth dopants with the host band states is of crucial importance for the potential spintronics applications. We analyze this by monitoring the exchange splitting, $\Delta E=\epsilon(\downarrow)-\epsilon(\uparrow)$, of the band states at the valence band maximum (VBM) and the conduction band minimum (CBM), both of which occur at the Γ point in the pure hosts as well as for the $x=1/16$ impurity supercells. Here the spin-direction $\uparrow$ is taken as the direction of the rare-earth spin (majority spin direction). At the VBM, the topmost $j=3/2$ fourfold degenerate valence state Γ_8 splits into four distinct energies separated by a few meV. Two of these are essentially pure spin-up and spin-down, respectively, (corresponding to the $m_j=\pm 3/2$ quantum numbers), and Fig. 6 shows the calculated differences in energy between these two states. The CBM state is the twofold Γ_6 state, which is antibonding s-like, and its splitting in the presence of magnetic rare-earth ions is depicted in Fig. 7

The spin-splitting of the top of the valence band in GaN is seen to peak around Nd at a value of 45 meV (Fig. 6), and falling smoothly towards a value of 6 meV in Yb. In contrast, the spin-splitting of the valence band of GaAs fluctuates more, which is due to the interaction with the unoccupied f-states. The latter appear in the SIC-LSD description as impurity bands, moving down with respect to the host bands, as one moves across the first half of the lanthanide series, and again similarly for the second half of the series. This is illustrated for GaN in Fig. 8. The hybridization effect of the f-bands with the VBM p-bands, as well as with the CBM s-bands, can be substantial[24] if the f-bands are close in energy to the gap edges.

In the case of GaAs the f-impurity band actually merges with the VBM for Sm and Eu dopants, while for Pm dopants the f-band is just above the VBM. Due to level repulsion the majority spin p-band at the VBM for GaAs:Pm is pushed significantly more down. Similarly, for the other spin channel in the second half of the lanthanide series, the f-band crosses

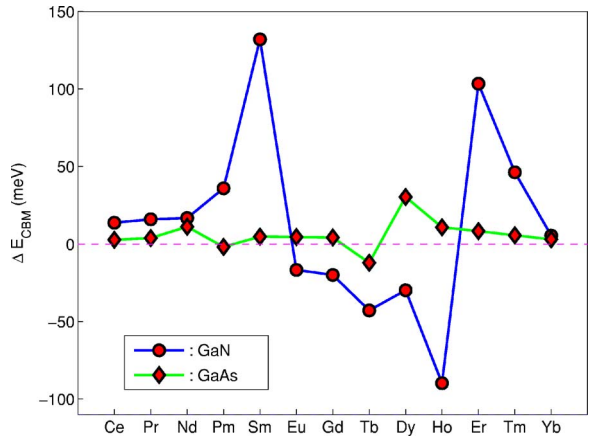

FIG. 7. (Color online) Spin-splitting (in meV) of the electron bands at the conduction band minimum for rare-earth dopants in GaN (circles) and GaAs (diamonds) for $x=1/16$. A positive sign implies that the band state with its spin aligned with the rare-earth spin has a lower energy than the state with its spin antiparallel to that of the rare-earth ion. The sign changes of the spin-splitting at the conduction band minimum around Sm and Ho are caused by the unoccupied rare-earth impurity f-bands crossing the conduction edge (cf., Fig. 8). Note the larger energy scale compared to Fig. 6.

the VBM between Ho and Er, and for Yb the f-like eigenvalue at the Γ-point is below the four-fold degenerate host VBM states (but only at Γ, the impurity band is about one-third filled at self-consistency).

The sign of the spin-splitting at the top of the valence band is in all cases, except Ho in GaAs, positive, i.e., the VBM p-states tend to align with the rare-earth spin. Holes

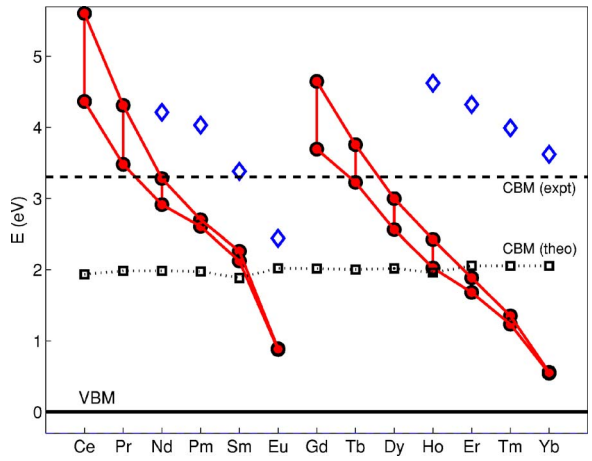

FIG. 8. (Color online) Trends in energy band structure around the fundamental gap for $RE_xGa_{1-x}N$, $x=1/16$, supercells. The VBM is at zero energy, full circles mark the unoccupied f-bands, while the squares and dotted line mark the calculated CBM. The f-band is defined by the smallest and largest f-dominated eigenvalue at the Γ-point (considering majority spin only, for the first half of the rare-earth series), and its width is mainly due to spin-orbit splitting. The experimental gap (3.3 eV) is marked with a dashed line. The calculated gap (for pure GaN) is 1.77 eV. The diamonds mark the calculated positions of the $\epsilon(0/-)$ levels in the localized picture, cf. Table I and Sec. III C.

will therefore predominantly be created in the minority spin channel, i.e., the p-type carriers will be spin-aligned with the rare-earth dopant. A similar small interaction was found for Gd in GaN in Ref. 24, which did not include spin-orbit interaction. However, in that work the opposite sign of the spin-splitting was reported. The origin of this sign difference most probably lies in the different treatment of the occupied Gd f-states. In Ref. 24 the f-states are treated as band states, which fall inside the occupied valence bands and interact strongly with the valence band top states. The repulsion effect on the majority spin states at the VBM is so strong that these are pushed above the minority VBM state, leading to a sign change of ΔE.

In contrast to the rather modest spin-splitting obtained for the rare-earth dopants in the present work, for Mn in GaN and GaAs it is much stronger. The spin-splitting induced by the Mn localized spins has been calculated[11] by the SIC-LSD method to be $\Delta E=-0.55$ eV and -0.43 eV in GaN and GaAs (for $x=1/16$), respectively, i.e., one or two orders of magnitude larger (and of opposite sign) than the splittings shown in Fig. 6. For Mn in GaAs and GaN, the overlap of the Mn d-states (in particular those of t_2 symmetry) with the host states at the VBM is significantly larger than that of the rare-earth ions. Hence for a Mn impurity with localized bonding and Mn d dominated states, the highest state at the VBM becomes the antibonding host-t_2-Mn d bandlike resonance, which is pushed up. At the same time, in the minority channel a bonding host-t_2-Mn d resonance is formed and moving down in energy, altogether leading to a negative spin-splitting $\Delta E=\epsilon(\downarrow)-\epsilon(\uparrow)$.[11] The calculations reported in Ref. 11 did not include the spin-orbit interaction, but the conclusions of that work prevail when spin-orbit interaction is included.[44] In the case of rare-earth dopants the f orbitals are much better confined to the rare-earth site and their hybridizations are significantly weaker, so that the spin-splitting becomes dominated by the direct exchange between host-states and rare-earth site (described through the spin-dependent effective potential). The only exception occurs when the unoccupied f-bands accidentally fall close to the host band edges, as discussed. Hence we conclude that for a p-type GaAs or GaN host there will be a much weaker spin polarization effect induced on the hole carriers by rare-earth dopants than when transition metal dopants are used.

GaN is usually n-type, so it is more appropriate to investigate the rare-earth induced effects on the conduction band states. This is a more difficult matter, since the LDA bands of the unoccupied conduction states are known to be inaccurate. Most importantly, the fundamental gaps are seriously underestimated, but in some cases the entire shape of the conduction bands is in error, e.g., in GaAs.[45] In the present approximation, the GaAs and GaN band gaps are calculated to be 0.11 and 1.77 eV, respectively, as compared to the experimental values of 1.42 eV[46] and around 3.3 eV,[47] and to full-potential LMTO values of 0.21 eV[48] (see also Ref. 49) and 2.2 eV.[47] A further complication is the appearance of the unoccupied f-bands of the rare-earth dopant, which interact with the host conduction band states, in particular with the s-like CBM.[24] The physical meaning of these f-bands depends on whether the band picture applies for an f-like electron added onto the rare-earth ion, which is doubtful. For

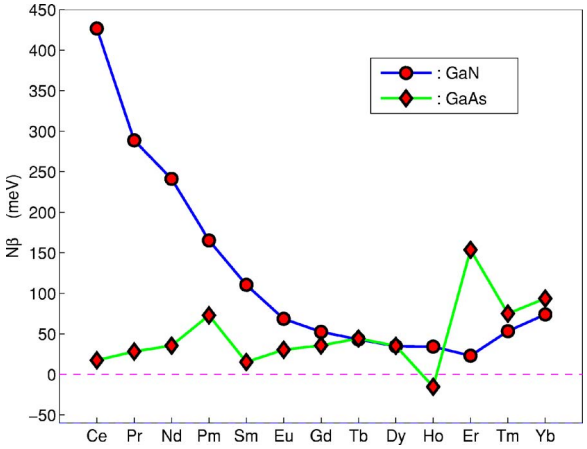

FIG. 9. (Color online) Exchange interaction parameter $N\beta$ of the valence band maximum for rare-earth dopants in GaN (circles) and GaAs (diamonds) for $x=1/16$.

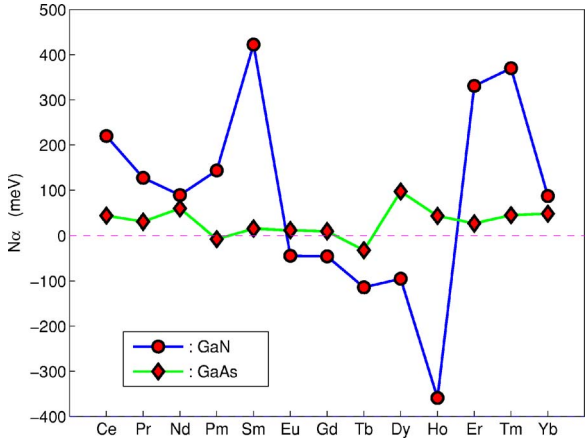

FIG. 10. (Color online) Exchange interaction parameter $N\alpha$ of the conduction band minimum for rare-earth dopants in GaN (circles) and GaAs (diamonds) for $x=1/16$.

example, the observation[15] of distinct multiplet lines in the photoluminescence spectra of rare-earth doped GaN clearly demonstrates the localized nature of the f-electrons. See also the discussion in the next section.

The spin-splitting of the CBM states seen in Fig. 7 is minute in GaAs, but much stronger in GaN, in particular where the unoccupied f-bands cross the CBM, which occurs around Sm and Ho (see Fig. 8). In the midlanthanide series, for Eu, Gd, Tb, Dy, and Ho, the exchange interaction is antiferromagnetic, i.e., the minority spin CBM state is lower than the majority spin state. This is again caused by the level repulsion effect. In the case of Eu, the unoccupied band of the seventh majority spin electron has moved below the conduction band edge thus pushing the majority spin s-state at CBM up. For Gd, Tb, Dy, and Ho, the unoccupied f-band states are of minority spin, and situated above the CBM, thus pushing the minority spin s-like CBM state down below the majority spin s-like CBM state. This behavior was also demonstrated for Gd in hypothetical zinc-blende GdN in Ref. 24.

To further analyze the exchange interaction of the rare-earth ion with the p-like VBM, the relevant exchange integral J_{pf} is extracted using the expression[50]

$$N\beta \equiv NJ_{pf} = \frac{\Delta E_{VBM}}{2Sx}. \tag{7}$$

Similarly, the exchange-splitting of the CBM s-like state can be quantified through an s-f interaction parameter:

$$N\alpha \equiv NJ_{sf} = \frac{\Delta E_{CBM}}{2Sx}. \tag{8}$$

In these expressions, S is the total spin of the rare-earth ion, x the dopant concentration, and N the number of host formula units within the normalization volume entering the definition of exchange integrals.[51] Figures 9 and 10 show the values of these parameters through the rare-earth series.

The exchange integral parameters are seen to reflect the behaviors already discussed for the spin-splittings in Figs. 6 and 7. For Gd in GaN we may compare to the exchange parameters extracted in Ref. 24 for GdN, whose estimated coupling parameters $N\beta=-0.01$ eV and $N\alpha=-0.4$ eV are showing somewhat weaker coupling to the VBM but significantly stronger coupling to the CBM, as compared to our respective values of $N\beta=53$ meV and $N\alpha=-46$ meV, calculated for the diluted Gd in GaN (see Figs. 9 and 10).

In contrast to the rather modest interaction parameters obtained for the rare-earth dopants here, for dilute Mn in GaN and GaAs, the exchange interaction of the Mn localized spins with the VBM was obtained as $N\beta=-2.5$ eV in GaN and $N\beta=-1.5$ eV in GaAs.[11]

In conclusion, it appears very unlikely that isolated rare-earth dopants by themselves can cause the room temperature ferromagnetism, let alone the giant magnetization amplifications, observed in the experiments by Ref. 14.

C. Acceptor levels

The behavior elucidated in Figs. 7 and 10 can only be considered a trend study, since the absolute positions of the conduction bands are not accurate. The LSD is known to substantially underestimate the band gap of semiconductors.[52] In the SIC-LSD approach the host band states are described by the LSD approximation, however, applied to the self-consistent charge density as obtained by the minimization of the SIC-LSD energy functional, Eq. (1), which deviates somewhat from the self-consistent charge density obtained by minimizing the LSD total energy functional. Generally, the SIC-LSD leads to larger magnetic moments and larger f-electron occupation than the LSD, although sometimes the difference can be rather small. Hence we may anticipate that the gap problem of LSD prevails in SIC-LSD.

Even more problematic is the description of the unoccupied f-states as weakly correlated LSD bands, which is in conflict with the localized picture used for the occupied part of the f-manifold. The LSD potential is derived from the limit of nearly-free electrons, i.e., fast electrons moving in an effective potential as given by the LSD approximation. This is a good approximation for most cases, e.g., for the occupied states of the host materials, which are built from ex-

tended *s*- and *p*-orbitals of the constituent atoms. The approximation is less adequate for the spatially confined *f*-orbitals of the rare-earth dopant, for which the overlap with neighboring impurity atoms is small. Hence an extra added *f*-electron would tend to stay for a long time on one rare-earth ion before hopping to a neighbor. The local environment will have time to adjust to the presence of the extra electron, and the effective potential will be modified. The same effect is well-known for localized gap states in semiconductors, for which the transition state approximation is often invoked, i.e., the defect energy level is calculated by occupying the defect state with half of an electron. In this section we will investigate various approaches to the calculation of the *f*-related acceptor levels $\epsilon(0/-)$ corresponding to the addition of one *f*-electron to the *f*-shell.

In the delocalized limit, as discussed, the added *f*-electron is put in the lowest unoccupied *f*-impurity band, which is positioned at

$$\epsilon_{LSD} = \langle f_{n+1} | H_{LSD} | f_{n+1} \rangle, \tag{9}$$

where $|f_{n+1}\rangle$ is the one-particle *f*-state, and H_{LSD} is the LSD Hamiltonian evaluated with the self-consistent charge density as obtained by minimization of the $E^{SIC\text{-}LSD}$ functional. Generally, several unoccupied *f*-states exist, and the lowest value of the above matrix element must be taken to represent the minimal addition energy.

In the opposite limit of localized *f* states one may calculate the position of the $\epsilon(0/-)$ level of a divalent rare-earth ion with one additional localized *f*-electron, by an SIC-LSD total energy difference:

$$\epsilon(0/-) = E(f^{n+1},-) - E(f^n,0). \tag{10}$$

Here, $E(f^n,0)$ is the total energy of the charge neutral trivalent rare-earth ion, while $E(f^{n+1},-)$ refers to the total energy of a divalent rare-earth ion with an extra electron in the supercell, and a homogeneous positive background charge of $+e$ added. In the approximation implied by Eq. (10) it is thus assumed that the presence of an extra electron on the rare-earth ion may be artificially compensated by the positive background charge, rendering the supercell altogether electrically neutral, which is necessary in order to have a well-defined total energy minimization problem. Obviously, spurious electrostatic interactions are introduced by this approach, and the reliability of the scheme must be checked. The same approach is often invoked for other charged impurities in semiconductors.[53,54]

A good test of the approximation in Eq. (10) is provided by the charge neutral SIC-LSD approximation for the *f* addition level. The latter is defined as the SIC-LSD total energy difference between divalent and trivalent rare-earth ions in a charge neutral supercell, i.e., the extra electron added to the rare-earth is supplied from the highest valence band state. This corresponds to the energy differences displayed by the *E*(*II*)-*E*(*III*) curve in Figs. 1 and 2:

$$\epsilon(0/-)_{appr} - \epsilon_{VBM} = E(f^{n+1},0) - E(f^n,0). \tag{11}$$

In this approximation the net accumulation of negative charge in the vicinity of the rare-earth ion is simply supplied from the Fermi level, however, due to the finite supercell, uncontrollable interactions between the negative *f*-ion and the hole state introduced will occur. The charge density of the host hole state does not correspond to a completely homogeneous charge density, and furthermore, the missing electron charge influences also the exchange-correlation part of the energy functional. Hence the two approaches differ, but as we will show give quite similar results, so that we can conclude that indeed the Coulombic interaction caused by the finite supercell is small.

Finally, we can also improve on the delocalized description of the *f* acceptor level by considering the transition state. The position of the lowest unoccupied *f*-band at half occupancy may be approximated as the average of the position of this band at zero and full occupancy:

$$\epsilon_{TS}^{+} = \frac{1}{2}[\epsilon_{LSD}(II) + \epsilon_{LSD}(III)]. \tag{12}$$

At zero occupancy, $\epsilon_{LSD}(III)$ corresponds to Eq. (9), and at full occupancy $\epsilon_{LSD}(II)$ corresponds to the same expression, however evaluated with the LSD Hamiltonian for the self-consistent charge density corresponding to the divalent rare-earth configuration. In this expression, $|f_{n+1}\rangle$ must be that particular *f*-state, which is delocalized in the trivalent but localized in the divalent configuration. The difference between the two LSD eigenvalues entering the average can be identified as an effective Coulomb *U* parameter, and the transition state energy is therefore equivalent to a shift by $\frac{1}{2}U$ of the LSD unoccupied band.

In Table I we compare for selected cases the *f*-related $\epsilon(0/-)$ level in Eq. (10) with the approximate expressions given by Eqs. (9), (11), and (12). The theoretical and experimental host gaps are quoted for comparison. The most consistent interpretation of the present results is to compare the calculated levels with the theoretical band gap, but often comparisons to the experimental gap in fact are done. After all, the band-gap discontinuity[52] problem persists in the expressions (10)–(12). One observes that in all cases the negatively charged rare-earth impurity has a higher energy than the theoretical band gap, and hence appears as a scattering resonance in the conduction bands. The implication is that even in *n*-type material the rare-earth ions will remain trivalent. If compared to the experimental band gap, only for Eu, Tm, and Yb in GaAs and for Eu in GaN does the $\epsilon(0/-)$ level fall below the experimental conduction band edge, while for Sm the $\epsilon(0/-)$ level comes rather close to the experimental conduction edge. Photoluminescence of (wurtzite) GaN:Eu thin films reveals no signature of divalent Eu ions,[39] thus corroborating the conclusions drawn in the present work if comparison to the theoretical gap is done.

Through the rare-earth series, the approximate expression in Eq. (11) differs from Eq. (10) by only 0.02–0.3 eV, which is reassuring, since it shows that the spurious charge interaction effects of the divalent rare-earth ion in the finite supercell are quite small. The correction with respect to the LSD band position is significant, generally several eV, i.e., the local Coulombic corrections due to the presence of the added localized *f*-electron are substantial. As explained, the transi-

TABLE I. Calculated defect levels of divalent rare-earth dopants in GaAs and GaN. The first column gives the host with experimental and theoretical gap values, the second column the dopant, the third column the calculated defect level on the basis of the SIC-LSD total energy difference, Eq. (10), the fourth column the same with the approximate expression, Eq. (11), i.e., neglecting the charging of the near defect region, the fifth column the LSD position of the lowest unoccupied f-band, Eq. (9), and the sixth coulmn the transition state as defined in Eq. (12). All numbers are in eV and relative to the VBM.

Host/gap	Dopant	$\epsilon(0/-)$	$\epsilon(0/-)_{appr}$	ϵ_{LSD}	ϵ^{+}_{TS}
	Pm	2.30	2.13	0.37	2.39
GaAs	Sm	1.47	1.28	0.13	1.96
	Eu	0.89	0.80	0.00	1.88
Expt.	Gd	4.17	4.20	1.71	4.98
1.42	Tb	3.25	3.23	0.61	3.13
	Ho	2.13	2.15	0.24	2.83
Theor.	Er	1.85	1.70	0.00	2.59
0.11	Tm	1.12	1.20	0.00	2.41
	Yb	0.89	0.97	0.00	2.38
	Nd	4.21	4.43	2.91	5.09
GaN	Pm	4.03	4.06	2.56	4.90
	Sm	3.38	3.11	2.12	3.69
Expt.	Eu	2.44	2.15	0.61	2.79
3.3	Ho	4.62	4.44	1.99	4.57
	Er	4.32	4.19	1.65	4.44
Theor.	Tm	3.99	3.89	1.17	4.37
1.77	Yb	3.62	3.45	0.57	3.78

tion state construction seeks to take this into account, and indeed brings the level position in much better agreement with the expression in Eq. (10), although it tends to mostly overshoot, in some cases by more than 1 eV.

D. f removal energies

The calculation of the energy position of the localized states in SIC-LSD theory has always been a matter of concern. The f removal energies one observes in photoemission include all the atomic multiplets of the f^{n-1} ion left behind, which can lead to a spectral function with f-related features over a $\sim$10 eV range.[19,55] Even calculating the energy of the most stable state with one f-electron removed is difficult. First of all, this will usually not be the ground state for an $N-1$ electron system, so applying a density functional theory based formalism poses a problem. But also in practice, the self-consistency process for a rare earth with a hole created in the f shell leads to unwanted effects, since the enhanced Coulomb attraction due to the missing f-electron will pull down the unoccupied f-levels below the Fermi level. Hence, if the initial state corresponds to a localized f^n configuration, the effective rare-earth configuration in the final state will not be f^{n-1}, but something in between f^{n-1} and f^n, often closer to the latter, and hence a too small removal energy is obtained (photoemission experiments do interprete certain features in terms of such "well screened" peaks[56]). On the other hand, just knocking out the f-electron but not driving the charge density to self-consistency overestimates the f removal energy by not allowing for screening of the charge hole by non-f electrons. What is physically relevant is an intermediate picture, where the fast non-f electrons are allowed to screen the charge hole, while the f-electrons are not allowed to respond to the removed charge, a situation which is not easily implemented in a total energy scheme.

According to Janak's theorem,[57] the derivative of the LSD energy functional with respect to orbital occupation is equal to the LSD eigenvalue for the corresponding orbital, which can be taken as a good representative of the removal energy of an electron in that state, if the charge of the orbital is everywhere small, as it will be for a bandlike state. A similar theorem holds in SIC-LSD,[58] where the SIC eigenvalue

$$\epsilon_{SIC} = \langle f | H_{LSD} + V_{SIC} | f \rangle \tag{13}$$

represents the derivative of the SIC-LSD total energy with respect to the occupation of the "canonical orbitals," which in the context of a periodic solid means a Bloch state formed from the localized f-states on all the rare-earth sites. Here, V_{SIC} represents the additional potential term arising in the self-consistency equation due to the self-interaction term in Eq. (4). Hence, using the SIC eigenvalues, the occupied f-states (without multiplets) appear as sharp resonances (SIC-LSD "bands"[58]) below the valence bands (at around -11.5 eV for the case of Eu in GaN depicted in Fig. 4), which is unrealistically deep for comparison to physical removal energies as observed in photoemission. The reason is that photoemission knocks out a localized f-electron rather than a "canonical" f-state.

Similar to the previous section, we may, however, apply a physically more reasonable but theoretically less rigorous approach by placing the removal energies of f-states at the transition state position. The eigenvalue given by Eq. (13) represents the energy cost due to removal of the first infinitesimal part of the f-electron (since V_{SIC} is evaluated for the initial ground state, i.e., at full occupancy), but as more and more of the f-electron is removed, the SIC potential term decreases, and eventually, only H_{LSD} is left. As an average we may therefore take the f removal energy as midway between the SIC-LSD and LSD band positions:

$$\epsilon^{-}_{TS} = \frac{1}{2}(\langle f | H_{LSD} + V_{SIC} | f \rangle + \langle f | H_{LSD} | f \rangle). \tag{14}$$

In effect, the SIC potential is only counted with half its strength in the transition state approximation to the removal energy. By evaluating H_{LSD} in the initial state, i.e., without the hole in the f shell, we avoid the aforementioned effect of the f-hole pulling the f levels down. The transition state philosophy was also implemented in Ref. 59, albeit in a different manner, by invoking the averaging factor of $\frac{1}{2}$ already in the total energy functional, while we do it here only for the removal energy, Eq. (14), after self-consistency.

Figure 11 displays the trends of ϵ^{-}_{TS} through the lanthanide series in both GaAs and GaN. The gradual increasing binding of the f-shell is clearly reflected in the transition state,

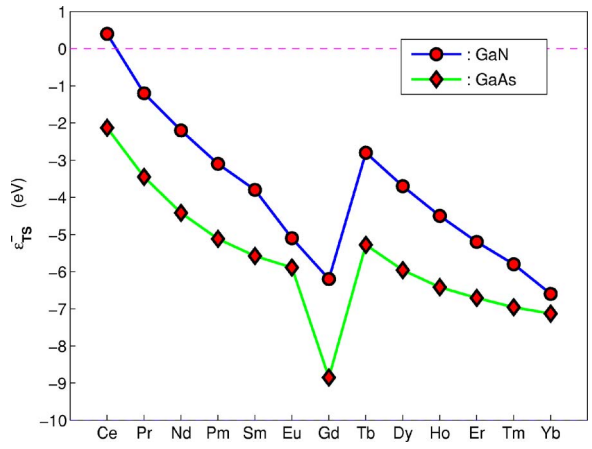

FIG. 11. (Color online) Transition state estimate, Eq. (14), of the f removal energies in GaAs (diamonds) and GaN (solid circles). The units are eV and relative to the VBM.

only broken at Gd in the middle of the series. Furthermore, the f removal energy is consistently smaller (less negative) in GaN compared to GaAs. A few experimental data corroborate the interpretation of the transition state as a good measure of the f removal energy: In Ref. 40 the photoemission spectra of Eu doped GaN reveal the signature of the $f^6 \rightarrow f^5$ transition in the interval between 5 and 10 eV below the Fermi edge, i.e., the lowest $f^5(^6H)$ multiplet is situated at −5 eV, in excellent agreement with the value of −5.1 eV in Fig. 11. For GdN films, the Gd f-emission peaks at −7.8 eV,[60] compared to the transition state energy of dilute Gd in GaN of −6.2 eV in Fig. 11. For YbN, the similar onset of f-emission is estimated to occur around −6 eV,[61] compared to the value −7.1 in Fig. 11. In CeAs, f-emission occurs around −2.5 eV,[19] as compared to the transition state estimate of −2.1 eV for dilute Ce in GaAs. In GdAs, f-emission occurs at −9 eV,[62] while the estimate of Fig. 11 for Gd in GaAs is −8.9 eV. For ErAs, the f-emission starts at −5 eV,[63] while the transition state position of dilute Er in GaAs is calculated as −6.7 eV.

IV. SUMMARY

Trends in the electronic structure of rare-earth substitutional impurities in GaAs and cubic GaN have been discussed based on self-interaction corrected local spin density calculations. The trivalent configuration is found as the ground state, while the divalent acceptor level is found above the theoretical band gap in all cases, and even above the experimental gap except for Eu, Tm, and Yb in GaAs and for Eu in GaN. However, the bare LSD eigenvalue is a poor approximation to this level, generally falling too low in the band gap, and in a few cases (Sm, Er, Tm, and Yb in GaAs) even closing the band gap completely. Instead, the proper localized nature of the $RE(2+)$ ion must be considered. Trends in f-electron removal energies were discussed based on transition state estimates showing a semiquantitative agreement with available experimental information.

The magnetic interaction of the rare-earth ion with the host states at the valence and conduction band edges has been investigated and found to be relatively weak in comparison with $3d$ impurities. Hence it is unlikely that the rare-earth dopant by itself may induce room-temperature ferromagnetism and gigantic magnetic enhancement, as observed in certain experiments.[14] To explain these experiments it seems imperative to include the interaction of the rare-earth dopants with other defects, native or external, which will be pursued in our future research.

ACKNOWLEDGMENTS

This work was partially funded by the EU Research Training Network (Contract No. HPRN-CT-2002-00295) "Ab-initio Computation of Electronic Properties of f-electron Materials." A.S. and N.E.C. acknowledge support from the Danish Center for Scientific Computing. A portion of this research was conducted at the Center for Nanophase Materials Sciences, which is sponsored at Oak Ridge National Laboratory by the Division of Scientific User Facilities, U.S. Department of Energy.

[1] S. A. Wolf, D. D. Awschalom, R. A. Buhrman, J. M. Daughton, S. von Molnar, M. L. Roukes, A. Y. Chtchelkanova, and D. M. Treger, Science **294**, 1488 (2001).
[2] I. Zutic, J. Fabian, and S. Das Sharma, Rev. Mod. Phys. **76**, 323 (2004).
[3] R. K. Kawakami, Y. Kato, M. Hanson, I. Malajovich, J. M. Stephens, E. Johnston-Halperin, G. Salis, A. C. Gossard, and D. D. Awschalom, Science **294**, 131 (2001).
[4] C. Liu, F. Yun, and H. Morkoç, J. Mater. Sci.: Mater. Electron. **16**, 555 (2005).
[5] A. H. Macdonald, P. Schiffer, and N. Samarth, Nat. Mater. **4**, 195 (2005).
[6] T. Dietl, H. Ohno, F. Matsukara, J. Cibert, and D. Ferrand, Science **287**, 1019 (2000).
[7] T. Jungwirth, J. Sinova, J. Mašek, J. Kučera, and A. H. MacDonald, Rev. Mod. Phys. (to be published 2006).
[8] P. Mahadevan and A. Zunger, Phys. Rev. B **69**, 115211 (2004).
[9] K. Sato, P. H. Dederichs, and H. Katayama-Yoshida, Hyperfine Interact. **160**, 57 (2005); K. Sato, H. Katayama-Yoshida, and P. H. Dederichs, Psi-K Newsletter **70**, 93 (2005).
[10] P. Sharma, A. Gupta, K. V. Rao, F. J. Owens, R. Sharma, R. Ahuja, J. M. O. Guillen, B. Johansson, and G. A. Gehring, Nat. Mater. **2**, 673 (2003).
[11] T. C. Schulthess, W. M. Temmerman, Z. Szotek, W. H. Butler, and G. Malcolm Stocks, Nat. Mater. **4**, 838 (2005).
[12] L. Petit, T. C. Schulthess, A. Svane, Z. Szotek, W. M. Temmerman, and A. Janotti, Phys. Rev. B **73**, 045107 (2006); L. Petit, T. C. Schulthess, A. Svane, W. M. Temmerman, Z. Szotek, and A. Janotti, J. Electron. Mater. **35**, 556 (2006).
[13] N. Teraguchi, A. Suzuki, Y. Nanishi, Y.-K. Zhou, M. Hashimoto,

and H. Asaji, Solid State Commun. **122**, 651 (2002).
[14] S. Dhar, O. Brandt, M. Ramsteiner, V. F. Sapega, and K. H. Ploog, Phys. Rev. Lett. **94**, 37205 (2005); S. Dhar, L. Perez, O. Brandt, A. Trampert, K. H. Ploog, J. Keller, and B. Beschoten, Phys. Rev. B **72**, 245203 (2005).
[15] A. J. Steckl, J. Heikenfeld, M. Garter, R. Birkhahn, and D. S. Lee, Compound Semicond. **6**, 48 (2000); U. Hömmerich, E. E. Nyein, J. Heikenfeld, A. J. Steckl, and J. M. Zavada, Mater. Sci. Eng., B **105**, 91 (2003).
[16] R. O. Jones and O. Gunnarsson, Rev. Mod. Phys. **61**, 689 (1989).
[17] R. M. Martin, *Electronic Structure* (Cambridge University Press, Cambridge, England 2004).
[18] P. Hohenberg and W. Kohn, Phys. Rev. **136**, B864 (1964); W. Kohn and L. J. Sham, Phys. Rev. **140**, A1133 (1965).
[19] M. Campagna, G. K. Wertheim, and Y. Baer, in *Photoemission in Solids II*, edited by L. Ley and M. Cardona (Springer, Berlin, 1979), Chap. 4.
[20] H. J. Lozykowski, W. M. Jadwisienczak, and I. Brown, J. Appl. Phys. **88**, 210 (2000).
[21] T. Andreev, N. Q. Liem, Y. Hori, M. Tanaka, O. Oda, Daniel Le Si Dang, and B. Daudin, Phys. Rev. B **73**, 195203 (2006).
[22] J.-S. Filhol, R. Jones, M. J. Shaw, and P. R. Briddon, Appl. Phys. Lett. **84**, 2841 (2004).
[23] B. Hourahine, S. Sanna, B. Aradi, C. Köhler, and T. Frauenheim, Physica B **376–77**, 512 (2006).
[24] G. M. Dalpian and S.-H. Wei, Phys. Rev. B **72**, 115201 (2005).
[25] J. P. Perdew and A. Zunger, Phys. Rev. B **23**, 5048 (1981).
[26] P. Strange, A. Svane, W. M. Temmerman, Z. Szotek, and H. Winter, Nature (London) **399**, 756 (1999).
[27] W. M. Temmerman, Z. Szotek, A. Svane, P. Strange, H. Winter, A. Delin, B. Johansson, O. Eriksson, L. Fast and J. M. Wills, Phys. Rev. Lett. **83**, 3900 (1999); A. Svane, W. M. Temmerman, Z. Szotek, L. Petit, P. Strange, and H. Winter, Phys. Rev. B **62**, 13394 (2000).
[28] W. M. Temmerman, H. Winter, Z. Szotek, and A. Svane, Phys. Rev. Lett. **86**, 2435 (2001).
[29] Z. Szotek, W. M. Temmerman, and H. Winter, Phys. Rev. Lett. **72**, 1244 (1994); A. Svane, *ibid.* **72**, 1248 (1994); M. Lüders, A. Ernst, M. Däne, Z. Szotek, A. Svane, D. Ködderitzsch, W. Hergert, B. L. Györffy, and W. M. Temmerman, Phys. Rev. B **71**, 205109 (2005).
[30] A. Svane, W. M. Temmerman, Z. Szotek, and H. Winter, Solid State Commun. **102**, 473 (1997); A. Svane, W. Temmerman, and Z. Szotek, Phys. Rev. B **59**, 7888 (1999).
[31] A. Svane, V. Kanchana, G. Vaitheeswaran, G. Santi, W. M. Temmerman, Z. Szotek, P. Strange, and L. Petit, Phys. Rev. B **71**, 045119 (2005).
[32] A. Svane, Phys. Rev. B **51**, 7924 (1995).
[33] A. Svane and O. Gunnarsson, Phys. Rev. Lett. **65**, 1148 (1990); Z. Szotek, W. M. Temmerman, and H. Winter, Phys. Rev. B **47**, R4029 (1993).
[34] O. K. Andersen, Phys. Rev. B **12**, 3060 (1975); O. K. Andersen and O. Jepsen, Phys. Rev. Lett. **53**, 2571 (1984).
[35] W. M. Temmerman, A. Svane, Z. Szotek and H. Winter, in *Electronic Density Functional Theory: Recent Progress and New Directions*, edited by J. F. Dobson, G. Vignale, and M. P. Das (Plenum, New York 1998), p. 327.
[36] J. Neugebauer and C. G. Van de Walle, Phys. Rev. B **50**, 8067 (1994).
[37] G. M. Dalpian and S.-H. Wei, Phys. Rev. Lett. **93**, 216401 (2004).
[38] P. H. Citrin, P. A. Northrup, R. Birkhahn, and A. J. Steckl, Appl. Phys. Lett. **76**, 2865 (2000).
[39] J. Heikenfeld, M. Garter, D. S. Lee, R. Birkhahn, and A. J. Steckl, Appl. Phys. Lett. **75**, 1189 (1999); E. E. Nyein, U. Hömmerich, J. Heikenfeld, D. S. Lee, A. J. Steckl, and J. M. Zavada, *ibid.* **82**, 1655 (2003).
[40] T. Maruyama, S. Morishima, H. Bang, K. Akimoto, and Y. Nanishi, J. Cryst. Growth **237–239**, 1167 (2002).
[41] H. Tanaka, M. Hashimoto, S. Emura, A. Yanase, R. Asano, Y.-K. Zhou, H. Bang, K. Akimoto, T. Honma, N. Umesaki, and H. Asahi, Phys. Status Solidi C **0**, 2864 (2003).
[42] H. J. Lozykowski, W. M. Jadwisienczak, and I. Brown, J. Appl. Phys. **88**, 210 (2000).
[43] M. Methfessel, Phys. Rev. B **38**, 1537 (1988).
[44] A. Svane *et al.* (unpublished).
[45] N. E. Christensen, Phys. Rev. B **30**, 5753 (1984).
[46] J. S. Blakemore, J. Appl. Phys. **53**, R123 (1982).
[47] N. E. Christensen and I. Gorczyca, Phys. Rev. B **50**, 4397 (1994).
[48] I. Gorczyca, N. E. Christensen, and A. Svane, Solid State Commun. **136**, 439 (2005).
[49] G. B. Bachelet and N. E. Christensen, Phys. Rev. B **31**, 879 (1985).
[50] B. E. Larson, K. C. Hass, H. Ehrenreich, and A. E. Carlsson, Phys. Rev. B **37**, 4137 (1988).
[51] G. D. Mahan, *Many-Particle Physics*, 2nd ed. (Plenum, New York, 1990).
[52] J. P. Perdew and M. Levy, Phys. Rev. Lett. **51**, 1884 (1983); L. J. Sham and M. Schlüter *ibid.* **51**, 1888 (1983).
[53] C. G. Van de Walle and J. Neugebauer, J. Appl. Phys. **95**, 3851 (2004).
[54] U. Gerstmann, P. Deak, R. Rurali, B. Aradi, Th. Frauenheim, and H. Overhof, Physica B **340**, 190 (2003).
[55] S. Lebègue, G. Santi, A. Svane, O. Bengone, M. I. Katsnelson, A. I. Lichtenstein, and O. Eriksson, Phys. Rev. B **72**, 245102 (2005).
[56] R. D. Parks, S. Raaen, M. L. denBoer, Y.-S. Chang, and G. P. Williams, Phys. Rev. Lett. **52**, 2176 (1984); D. M. Wieliczka, C. G. Olson, and D. W. Lynch, *ibid.* **52**, 2180 (1984).
[57] J. F. Janak, Phys. Rev. B **18**, 7165 (1978).
[58] M. R. Pederson, R. A. Heaton and C. C. Lin, J. Chem. Phys. **82**, 2688 (1985).
[59] A. Filippetti and N. A. Spaldin, Phys. Rev. B **67**, 125109 (2003).
[60] F. Leuenberger, A. Parge, W. Felsch, K. Fauth, and M. Hessler, Phys. Rev. B **72**, 014427 (2005).
[61] L. Degiorgi, W. Bacsa, and P. Wachter, Phys. Rev. B **42**, 530 (1990).
[62] H. Yamada, T. Fukawa, T. Muro, Y. Tanaka, S. Imada, S. Suga, D.-X. Li, and T. Suzuki, J. Phys. Soc. Jpn. **65**, 1000 (1996).
[63] T. Komesu, H.-K. Jeong, J. Choi, C. N. Borca, P. A. Dowben, A. G. Petukhov, B. D. Schultz, and C. J. Palmstrøm, Phys. Rev. B **67**, 035104 (2003).